Chapter 1

NV-NV cross-relaxations : the fluctuator model

This chapter will cover cross-relaxations between NV centers in the non-zero magnetic field regime, both from an experimental and theoretical point of view. The case of zero magnetic field will be treated in the next chapter.

The presence of strong NV-NV dipolar interaction in dense ensemble ([NV] $\gtrsim$ 1 ppm) proved to be both an obstacle for ensemble magnetometry [1] and an opportunity to explore and use the many-body interaction resulting from it [1–4].

We will see in this chapter how a model of fast and slow relaxing centers, the fluctuator model [5], explains most observations related to the cross-relaxation, including the stretched exponential lifetime profile and the spectral broadening of the interaction.

1.1 Experimental observation of NV-NV CR

Let us start with the experimental proof of the presence of NV-NV CR in the samples with dense NV ensembles.

When dealing with NV-NV CR, we have to make the distinction between what we will label "equivalent" and "non-equivalent" NV centers. Two equivalent centers are NV centers with the same spin Hamiltonian ([REF] chap 1), which implies that they both see the same transverse and longitudinal magnetic field. In contrast, non-equivalent centers are center with different single-spin Hamiltonian, which may result in different eigenstates and spin polarization for the two spins.

While the NV physics can explain cross-relaxations between non-equivalent NV centers, it cannot explain cross-relaxation between equivalent NV centers. Nevertheless, as we will see in this section, CR between both equivalent and non-equivalent NV centers is observed for samples with high NV density.

1.1.1 NV-NV CR between nonequivalent NV centers

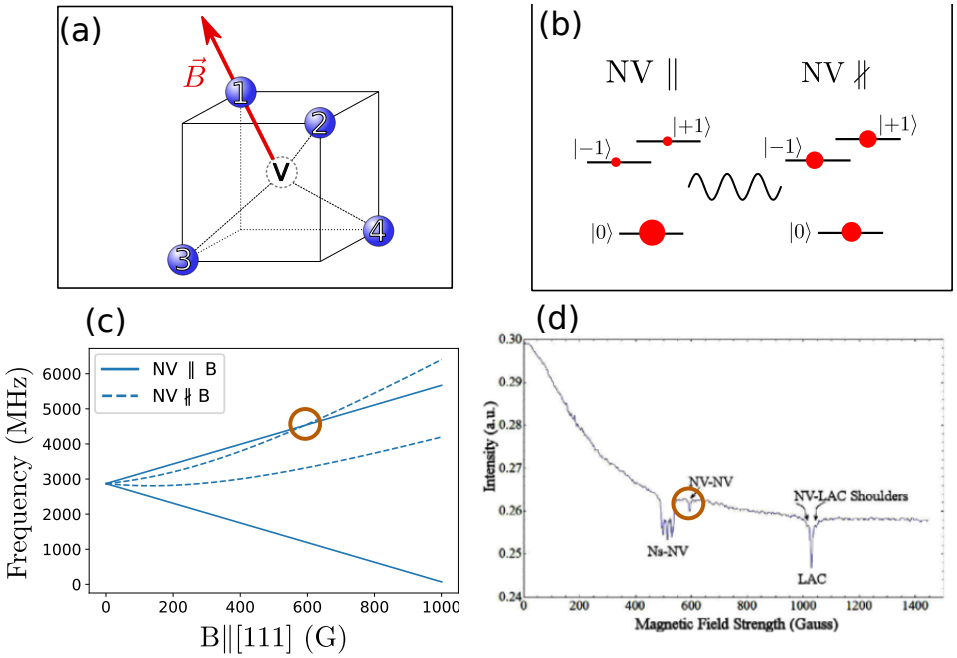

Figure 1.1: a) Illustration of the four possible direction of the the NV axis (four classes of NV centers) with a magnetic field along class 1 b) Representation of the polarization of two non equivalent spins, one aligned with the magnetic field (well polarized) and one misaligned with the magnetic field (unpolarized). c) Simulated frequencies for the $|0\rangle \rightarrow |-1\rangle$ and $|0\rangle \rightarrow |+1\rangle$ transitions when $\mathbf{B} \parallel [111]$ for the class aligned with B, and the 3 equivalent classes not aligned with B. d) Taken from [6], PL change of an ensemble of NV centers as a magnetic field is scanned along the [111] axis.

In the absence of magnetic gradient, two NV centers can only be non-equivalent if the projection of the magnetic field upon their respective NV axis is different. Fig. 1.1-a) illustrates such a case: we label here the four possible NV axis orientation (or NV classes) 1 to 4 and we assume that the magnetic field is aligned with class 1. In this conditions, an NV center belong to class 1 will always be non-equivalent with NV centers from classes 2-4, as the projection of the magnetic field on their respective axis will never be the same. On the other hand, NV centers from the classes 2-4 are all equivalents, even though they do not necessary belong to the same class.

Fig. 1.1-b) shows the difference between the NV centers belonging to class 1 labeled $NV_{\parallel}$) and those belonging to classes 2-4 (labeled $NV_{\nparallel}$). As explained in [REF], the transverse magnetic field leads to a mixing of the

eigenstates [1] and to a loss of the optical polarization mechanism. As a result, the $NV_{\nparallel}$ spins are less polarized than the $NV_{\parallel}$ ones, which is a necessary condition to observe cross-relaxation.

Another necessary condition to observe cross-relaxation is the condition of co-resonance. In most situations, non-equivalent NV centers are not co-resonant, as the differences in the spin Hamiltonian generally leads to different eigenvalues. This is in contrast with equivalent NV centers which are by definition always resonant. Fig. 1.1-c) shows the transition frequencies of spin from class 1 and a spin from class 2-4 as a function of the magnetic field amplitude. Unintuitively, there is a co-resonance between the two $|0\rangle \rightarrow |+1\rangle$ transitions for $|\mathbf{B}| = 592$ G. For this particular value of the magnetic field, cross-relaxation between the NV centers from class 1 and those from classes 2-4 is possible.

Finally, Fig. 1.1-d), which was presented in the last chapter, shows the experimental value of the total NV PL as a function of the magnetic field amplitude, in a scenario similar to the one we just described. We can indeed observe the signature of NV-NV CR in the presence of a PL dip at $|\mathbf{B}| = 592$ G.

As previously mentioned, cross-relaxation between non-equivalent NV centers is easily explained by the physics of single NV centers, and has been known for more than thirty years [7, 8].

1.1.2 NV-NV CR between equivalent NV centers

More recently, experiments on dense NV ensemble ([NV] $>$ 1 ppm) or at low temperature have shown that there were cross-relaxations even between equivalent NV centers [5, 9–11].

Fig. 1.2-a) illustrates the two possible scenarios for equivalent NV centers: either two NVs from the same class, or two NVs from different classes with the same projection of the magnetic field upon their respective axis (i.e. $\mathbf{B}$ belongs to the plane of mirror symmetry of the two spins).

In the second case, by moving the magnetic field in and out of the symmetry plane, we can change the resonance condition between the two NV classes and measure the contribution of NV-NV cross-relaxation to the NV PL and spin lifetime. To do so, we need to add an initial bias magnetic field in addition to the scanned magnetic field, as represented in Fig. 1.2-b).

Fig. 1.2-c) shows the transition frequencies of the $|0\rangle \rightarrow |-1\rangle$ transition for the 4 classes of NV centers on sample ADM-15-1, an HPHT microdiamond with [NV] ~ 3 ppm. There are three magnetic field values $B_{\text{scan}} \approx$ 12, 42 and 77 G for which there is an inter-class resonance. These values are reported in the figure with red dotted lines. Unlike the case presented

[1] The states of the misaligned NV on Fig. 1.1-b) are labeled $|0\rangle, |\pm 1\rangle$ which is an abusive (but common) notation since the mixing caused by the transverse field means that the eigenstates of S_z are no longer the Hamiltonian eigenstates.

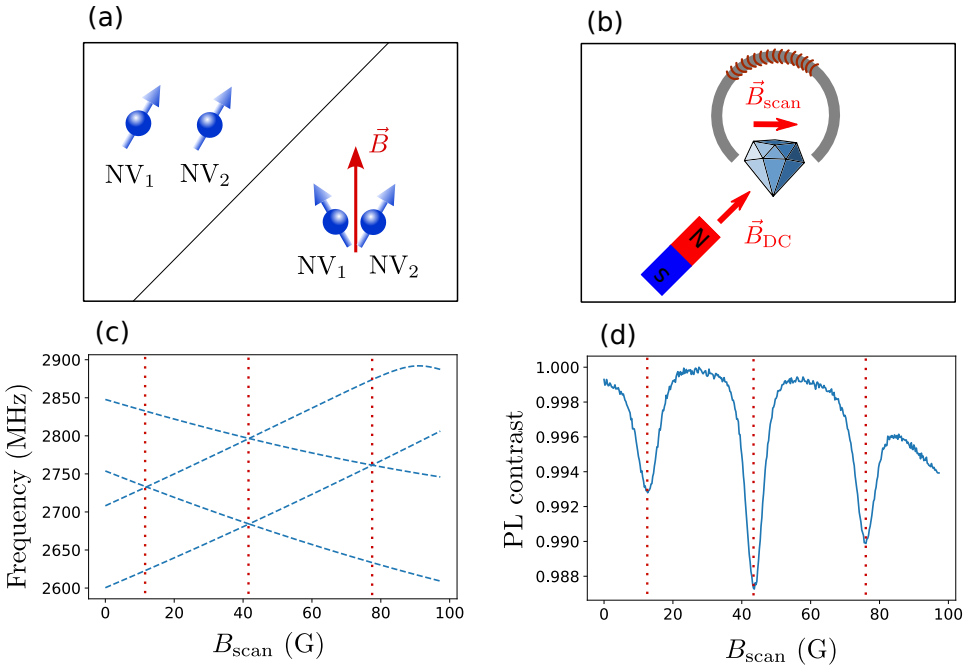

Figure 1.2: CR between equivalent NV centers for sample ADM-15-1. (a) Representation of equivalent NV centers: either two NVs from the same class, or two classes with the same projected magnetic field. (b) Magnetic setup used for the experiment: a permanent magnet is used to apply a bias magnetic field, and an electromagnet is used to add a variable magnetic field. (c) Simulation showing the $|0\rangle \rightarrow |-1\rangle$ transition frequencies for the 4 classes of NV centers as a function of the scanned magnetic field. The transitions were computed based on ODMR spectra recorded for different magnetic field values. (d) Change in the PL of the NV centers ensemble as a function of the scanned magnetic field.

in Fig. 1.1, all the inter-class resonances reported in Fig. 1.2-c) are between equivalent classes.

Finally, Fig. 1.2-d) shows the PL contrast as the electromagnet field is scanned. There are 3 very clear dips when $B_{\text{scan}} \approx 12$, 42 and 77 G which coincide with inter-class resonances. We will see later that this PL dip is associated with a decrease of the NV centers spin T_1 time from both classes.

This observation, and similar ones made by many groups [5, 9, 10, 12, 13], seem to indicate that there are CR between equivalent NV centers. This is however incompatible with our previous assumptions that equivalent NV centers are equally polarized and bright. To understand this phenomenon, we will need to introduce new hypotheses.

1.2 NV inhomogeneity and the fluctuator model

1.2.1 CR in an inhomogeneous NV bath

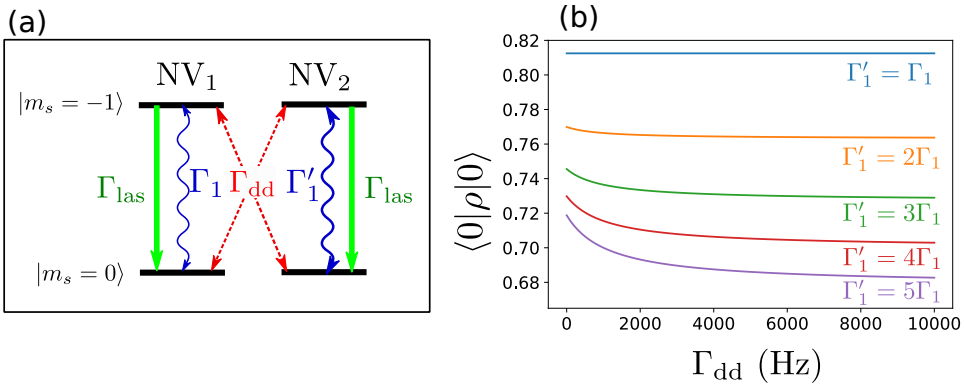

Figure 1.3: a) Schematics of the model: we consider a four level system consisting of 2 levels of 2 NV centers resonantly coupled through the flip-flop rate Γ_{dd}. These two NV centers are each pumped in their respective $|0\rangle$ state via the green laser with a rate Γ_{las}, and have their own relaxation rate Γ_1 and Γ_1^* respectively. b) Average population of the two NV centers in the $|0\rangle$ state in the steady state as a function of Γ_{dd} and Γ_1^*. The steady state was computed by solving a classical rate equation where we fixed $\Gamma_{las} = 1000$ Hz and $\Gamma_1 = 300$ Hz.

A likely explanation to the observed NV-NV CR is that the NV centers are not all equivalents.

Indeed, if we assume that, for instance, the relaxation rate $\Gamma_1 = 1/T_1$ is not strictly the same for each NV centers, but instead follows a certain distribution $\rho(\Gamma_1)$, then CR between NV centers with different Γ_1 can explain the observations in Fig. 1.2.

Fig. 1.3-a) and b) illustrates this case. Our model here consists of two (resonantly coupled) NV centers with two different relaxation rates Γ_1 and Γ_1'. To complete the model, we add the rate Γ_{las} which is the optical pumping rate from the $|-1\rangle$ to the $|0\rangle$ state of each spin, and Γ_{dd} the flip-flop rate between the two spins [2]. We only consider here the incoherent dynamics of the population, modeled with the rates reported on Fig. 1.3-a). Solving for the steady state of these rate equations, we can compute the final population in the $|0\rangle$ state for both spins.

Fig. 1.3-b) shows the spin population in the $|0\rangle$ state of both spins, ρ_{00}, as a function of the flip-flop rate Γ_{dd} and for various values of Γ_1'. The first thing to notice is that, as Γ_1' is increased, ρ_{00} decreases. This is because NV_2

[2] We consider here a two level system instead of the full three levels of the spin 1. The choice of $|-1\rangle$ instead of $|+1\rangle$ is arbitrary.

becomes less polarized as its decay rate increases. The second thing to notice is that, when $\Gamma_1' = \Gamma_1$, i.e. when the two NV centers are truly equivalent, the flip-flop rate has no incidence on ρ_{00}. However, when $\Gamma_1' > \Gamma_1$, ρ_{00} decreases when the flip-flop rate increases. Intuitively, this can be thought of as NV_2 acting as a polarization drain on NV_1.

We can also notice that the influence of the flip-flop rate on ρ_{00} increases when the difference in decay rates between NV_1 and NV_2 increases. As a result, we can suppose that a greater inhomogeneity between the NV centers would result in a stronger NV-NV cross-relaxation effect.

1.2.2 Presentation of the fluctuator model

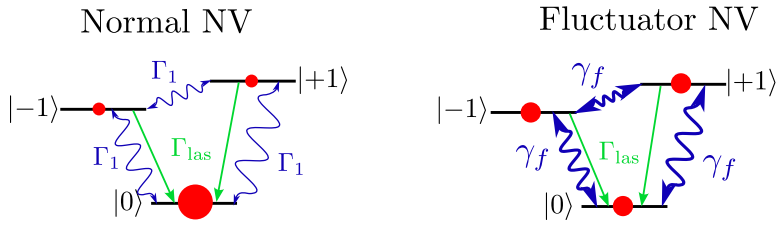

Figure 1.4: Representation of a "normal" NV center with spin depolarization rate $\Gamma_1 \ll \Gamma_{\text{las}}$ and a fluctuator NV with spin depolarization rate $\gamma_f \gg \Gamma_{\text{las}}$. Red circles represent the spin population in the steady state of each spin

Choi et al. in [5] take this approach a step further by separating the NV centers into two groups: "normal" NV centers with a phonon-limited lifetime outside of dipole-dipole interaction, and "fluctuators" which are NV centers with an intrinsic, extremely fast relaxation mechanism leading to a new depolarization rate γ_f. Normal and fluctuator NV are represented in Fig. 1.4: in their model, Choi et al. assume that the fluctuator decay rate is fast enough compared to the laser polarization rate $\gamma_f \gg \Gamma_{\text{las}}$ that the fluctuators are effectively always depolarized. Fluctuators are therefore similar to the dark spins we introduced in the last chapter.

We should note here that, while this simplifications seem a bit extreme, the fluctuator model is more than a toy model. There are good evidence of the presence of these dark NV centers in dense NV ensemble, as will be discussed below.

In their model, the authors of [5] consider that the fluctuators act as a Markovian bath, meaning that the fluctuator density matrix will always read $\rho = \frac{1}{3}I$, regardless of its interaction with NV centers. With this assumption, the modification caused by the fluctuator bath on the "normal" NV lifetimes can be analytically computed.

Other possibilities to explain the change in the relaxation rate were considered, such as spin diffusion to non-polarized NV centers (outside of the

laser spot) or phonon superradiance, but they were not considered to be viable explanations: spin diffusion is orders of magnitude too slow to explain this phenomenon [5], and the NV-NV CR seem to be independent of the crystal temperature [9, 10] which is incompatible with phonon superradiance [5].

Before detailing the model's predictions, we will first contemplate the possible microscopic origin of these fluctuators, and review some physical systems were similar observations have been made.

1.2.3 Possible microscopic origin of the fluctuators

We should note first that a similar problem of spin ensemble relaxation rate increasing with the spin concentration was observed more than six decades ago with phosphorus doped silicon [14, 15]. It was proposed that the cause of the relaxation was the presence of fast relaxing centers coupled to the slow relaxing centers through spin diffusion [15–19].

This conclusion was based on previous observations on the relaxation of nuclear spins [20–22], where some nuclear spins had a considerably reduced lifetime due to their proximity to paramagnetic ions. Similar observations were performed with Förster resonant energy transfer (FRET) in chromophore molecules [23–25], where excited donor molecules are coupled through (electric) dipole-dipole interaction to non-excited acceptor molecules.

In the case of P-doped Si, the origin of the fast relaxing centers is thought to be closely packed P impurities, so that the electronic wavefunctions of (at least) two P centers overlap. In that case two phenomena occur: the possibility of electron tunneling, and the apparition of a contact interaction term in the dipole-dipole Hamiltonian (see appendix [REF]). Both of these phenomena can lead to fast spin relaxation: electron tunneling can be accompanied by a spin reversal [16], and the modulation of the contact interaction term ($J-$coupling) by the crystal phonons can directly excite the spin transitions [15]. While the dipole-dipole interaction terms (excluding the contact interaction) are also modulated by the phonons, this effect would be too small to account for the fast depolarization observed here.

Similarly, [5] suggests that the origin of fluctuators in NV centers are closely packed NV centers or NV-impurity pairs which undergo rapid electron hopping and spin depolarization. To prove their point, they look at the charge dynamics in their sample and find that there is charge recombination in the dark with a corresponding tunneling rate between neighboring sites of ~ 10 ns. In contrast to P-doped Si, the NV centers are not the most abundant electronic defects in the crystal, this is why the $NV^- - N^+$ pair in particular is thought to be a likely candidate for the fluctuators [26].

1.2.4 Single NV center coupled to a single fluctuator

We now turn to the computation of the depolarization induced by the fluctuator bath on the NV centers. We will follow here the notations and calculation steps in [5].

Let us first consider the interaction between a single NV center and a fluctuator. Since we assume the fluctuators to be always depolarized, this step is similar to the coupling of an NV center to a dark spin done in the last chapter.

We will first decompose the dipole-dipole Hamiltonian as a product between radial and angular part:

$$\mathcal{H}_{\text{dd}} \approx -\frac{J_0}{r^3}\left[(g+ih)(|0,+1\rangle\langle+1,0| + |0,-1\rangle\langle-1,0| + qS_z^1S_z^2\right] + h.c., \quad (1.1)$$

where the expression of J_0, g, h and q is given in appendix [REF]. g, h and q are dimensionless factors that are function of the relative radial positions and orientation of the two dipoles.

We then introduce the dimensionless number η defined as:

$$\eta^2 = \frac{1}{3}(|g|^2 + |h|^2)\frac{4\gamma_f^2}{(\omega_f - \omega_{NV})^2 + 4\gamma_f^2}, \quad (1.2)$$

where γ_f is the fluctuator decay rate for each possible channel between $|0\rangle, |-1\rangle$ and $|+1\rangle$. This number η encapsulates both the angular dependency (through g and h) and the resonance condition between the NV center and the fluctuator.

We can note that the spectral response of a single fluctuator, for which we only consider the broadening caused by the decay rate γ_f, is a Lorentzian of half width $2\gamma_f$. This is different from the usual lifetime limited optical spectra which are Lorentzian of half width $1/2T_1 = \Gamma_1/2$. The difference comes here from the fact that we consider thermalization going both ways (i.e. $|e\rangle \to |g\rangle$ and $|g\rangle \to |e\rangle$ instead of only $|e\rangle \to |g\rangle$) and that each state of the fluctuator can decay into two other states (see Fig. 1.4).

Finally, one finds that the additional depolarization rate induced by the fluctuator on the NV center reads:

$$\gamma_s(\mathbf{r}) = \left(\frac{J_0}{r^3}\right)\frac{\eta^2}{\gamma_f}. \quad (1.3)$$

Compared to eq. [REF], the dependency on the inhomogeneous broadening of the spins $1/T_2^*$ is hidden in the η factor, and we have the additional broadening γ_f coming from the fluctuators very short lifetime.

1.2.5 Ensemble of NV centers coupled to a bath of fluctuators

The next step is to compute the depolarization caused by the ensemble of fluctuators on a single NV center.

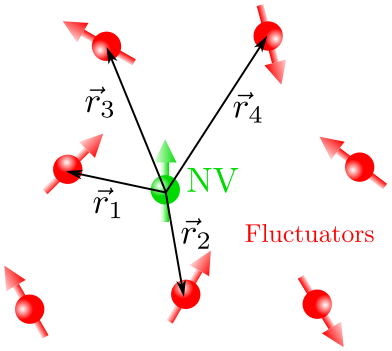

Figure 1.5: Schematics of an NV center in a fluctuator bath. The $\mathbf{r}_i$ vector represent the relative of position of fluctuator i with respect to the NV center.

We consider the situation pictured in Fig. 1.5: the NV center is at the center of the frame and the position of each fluctuator is labeled $\mathbf{r}_i$. We consider that each fluctuator is an independent depolarization source, therefore the depolarization on a single NV center reads:

$$\gamma = \sum_i \gamma_s(\mathbf{r}_i). \tag{1.4}$$

We then want to compute the distribution $\rho(\gamma)$ defined as:

$$\rho(\gamma) = \int d\{r_i\}\rho(\{r_i\})\,\delta\left(\sum_i \gamma_s(\mathbf{r}_i) - \gamma\right). \tag{1.5}$$

To do so, we need to determine the distribution of the fluctuators positions and orientations$\{r_i\}$. Assuming that they are homogeneously distributed in the bulk of the material, we find:

$$\rho(\gamma) = \frac{e^{-1/(4\gamma T)}}{\sqrt{4\pi\gamma^3 T}}, \tag{1.6}$$

where the time constant T was introduced and is defined as:

$$\frac{1}{T} = \left(\frac{4\pi n_f J_0 \bar{\eta}}{3}\right)^2 \frac{\pi}{\gamma_f}, \tag{1.7}$$

with n the fluctuator density and $\bar{\eta}$ the averaged value of $|\eta|$:

$$\bar{\eta} = \int \mathrm{Prob}(\eta)|\eta|\mathrm{d}\eta. \tag{1.8}$$

Finally, the polarization dynamics from the ensemble of NV centers can be computed:

$$P(t) = \int_0^\infty \rho(\gamma)\, e^{-\gamma t} d\gamma = e^{-\sqrt{t/T}}. \tag{1.9}$$

In conclusion, the fluctuators causes a depolarization on the NV ensembles with a timsecale T given by 1.7, and the dynamics of this depolarization is that of a stretched exponential [3], unlike the phonon-induced depolarization which is purely exponential.

It should be noted that the stretched exponential nature of the decay is not specific to the fluctuator model, but results from localized noise sources, randomly distributed in the bulk (3D). Indeed, [27] came to the same conclusion by analyzing the resonant coupling of NV centers with a P1 bath. Theodor Förster in 1949 also predicted and observed stretched exponential dynamics in the context of FRET, where the same scaling laws are observed [23].

1.2.6 Computation of $\bar{\eta}$

The parameter $\bar{\eta}$ in eq. (1.7) is of crucial importance as it encapsulates the resonance condition between the NV centers and the fluctuators. This resonance condition, i.e. the spectral overlap between the fluctuators and the NV centers, can be decomposed in two essential parameters: one is the central frequency of each subgroup (ω_{NV}^0 and ω_f^0 respectively) which themselves depends on the magnetic field, the other is the spectral broadening of both the NV and the fluctuators.

The aim of this section is to give an explicit formula of $\bar{\eta}$ as a function of ω_{NV}^0, ω_f^0 and T_2^*.

We will start by separating the factor η given in eq. (1.2) into a a geometric and a spectral part:

$$\eta^2 = G^2(\{\theta\})R^2(\omega_f, \omega_{NV}), \tag{1.10}$$

$$G^2 = \frac{1}{3}\left(|g|^2 + |h|^2\right), \tag{1.11}$$

$$R^2(\omega_f, \omega_{NV}) = \frac{4\gamma_f^2}{(\omega_f - \omega_{NV})^2 + 4\gamma_f^2}. \tag{1.12}$$

G is a function which depends purely on the various angles of the problem $\{\theta\}$, while R represents the resonance condition between the NV and the fluctuator.

We then average the η factor for an ensemble of fluctuators and NV

[3] Stretched exponential generally refer to functions of the form $\exp\left(-(t/\tau)^\beta\right)$. In this manuscript, unless specified otherwise, we will always refer to the case $\beta = 1/2$ when mentioning stretched exponential.

centers:

$$\begin{aligned}\bar{\eta} &= \int \mathrm{Prob}(\eta)|\eta|\mathrm{d}\eta \\ &= \left(\int \rho(\{\theta\})|G(\{\theta\})|d\{\theta\}\right) \\ &\times \left(\int \rho(\omega_{NV})\rho(\omega_f)|R(\omega_f,\omega_{NV})|d\omega_{NV}d\omega_f\right) \\ &= \bar{G}\cdot\bar{R},\end{aligned}$$

where we introduced $\rho(\{\theta\})$ the probability distribution of the angles $\{\theta\}$, $\rho(\omega_{NV})$ the inhomogeneous spectral distribution of the ensemble of NV centers and $\rho(\omega_f)$ the inhomogeneous spectral distribution of the ensemble of fluctuators. We also introduced the notations $\bar{G}$ and $\bar{R}$ as the average of $|G|$ and $|R|$.

The computation of $\bar{G}$ will be further discussed in sec. 1.4.2 and in appendix [REF]. We will focus here on $\bar{R}$.

To perform the computation, we need to know the distributions $\rho(\omega_{NV})$ and $\rho(\omega_f)$. We can experimentally measure $\rho(\omega_{NV})$ though ODMR, and we can reasonably expect $\rho(\omega_f)$ to follow the same probability.

We unfortunately cannot analytically solve for $\bar{R}$ with standard distributions of $\rho(\omega_f)$ and $\rho(\omega_{NV})$ (either Gaussians or Lorentzians). We can however solve for $\overline{R^2}$, which is close to $(\bar{R})^2$ as long as $2\gamma_f \gg 1/T_2^*$.

For a Lorentzian profile of $\rho(\omega_f)$ and $\rho(\omega_{NV})$ defined as:

$$\begin{aligned}\rho(\omega_f) &= \frac{1}{\pi\Gamma_f}\frac{1}{1+\left(\frac{\omega_f-\omega_f^0}{\Gamma_f}\right)^2} \\ \rho(\omega_{NV}) &= \frac{1}{\pi\Gamma_{NV}}\frac{1}{1+\left(\frac{\omega_{NV}-\omega_{NV}^0}{\Gamma_{NV}}\right)^2},\end{aligned}$$

where $\Gamma_f = 1/T_2^*(\text{fluctuator})$ and $\Gamma_{NV} = 1/T_2^*(\text{NV})$ are the inhomogeneous broadening of the NV and fluctuator ensembles, and ω_{NV}^0 and ω_f^0 are the central angular frequencies of the NV and fluctuator ensembles. We then find that:

$$\begin{aligned}\overline{R^2} &= \int \rho(\omega_{NV})\rho(\omega_f)\frac{4\gamma_f^2}{(\omega_f-\omega_{NV})^2+4\gamma_f^2}d\omega_{NV}d\omega_f \\ &= \frac{2\gamma_f}{2\gamma_f+\Gamma_f+\Gamma_{NV}}\cdot\frac{1}{1+\left(\frac{\omega_{NV}^0-\omega_f^0}{2\gamma_f+\Gamma_f+\Gamma_{NV}}\right)^2}.\end{aligned}$$

In the case where $\omega_{NV}^0 = \omega_f^0$, meaning that either the considered NVs and fluctuators are from the same class, or from two classes perfectly resonant, by substituting $\overline{R^2}$ for $(\bar{R})^2$ (which again is only approximately valid for $2\gamma_f \gg 1/T_2^*$) in eq. 1.7, we find that:

$$\frac{1}{T} \propto \frac{1}{2\gamma_f + \Gamma_f + \Gamma_{NV}} \cdot \frac{1}{1 + \left(\frac{\omega_{NV}^0 - \omega_f^0}{2\gamma_f + \Gamma_f + \Gamma_{NV}}\right)^2}. \tag{1.13}$$

If $\rho(\omega_f)$ and $\rho(\omega_{NV})$ follow Gaussian profiles instead, $\overline{R^2}$ is the integral of a Voigt profile, the convolution of a Lorentzian and a Gaussian, which does not have a clear analytic solution.

Eq. 1.13 was obtained via several approximations: the inhomogeneous distribution of the NV centers is generally not Lorentzian, and $\overline{R^2} \neq (\bar{R})^2$ in the general case. Nevertheless, it gives us a general idea of the evolution of $1/T$ with T_2^*, ω_{NV}^0 and ω_f^0, which will be crucial to compare the predictions of the model with experimental data.

1.3 Experimental investigation of the fluctuator model

We will now show experimental results related to the predictions of the fluctuator model.

1.3.1 The stretched exponential lifetime

The first prediction of the fluctuator model which can be experimentally verified is the stretched-exponential profile of the spin relaxation. The protocol to measure spin relaxation with a common mode rejection was presented in [REF].

Fig. 1.6 shows the results of this protocol on two distinct samples and magnetic field configurations. In both cases, we show the results in linear and logarithmic scale as the log scale makes deviations from the standard exponential more apparent[4].

The spin relaxation results presented in Fig. 1.6-a) and b) was performed on sample CVD-pink ([REF]), which despite a relatively high NV concentration shows only moderate amount of dipole-dipole spin relaxation. In order to further minimize the amount of cross-relaxations, we chose a magnetic field for which all four NV classes are spectrally isolated, so that only fluctuators from the same class as the NV center could lead to relaxation. As a result, we can see a relaxation profile mostly exponential with a

[4]The fits presented in Fig. 1.6 and in the next figures were performed by fitting the real value of $S_1 - S_2$ and not $\log(S_1 - S_2)$.

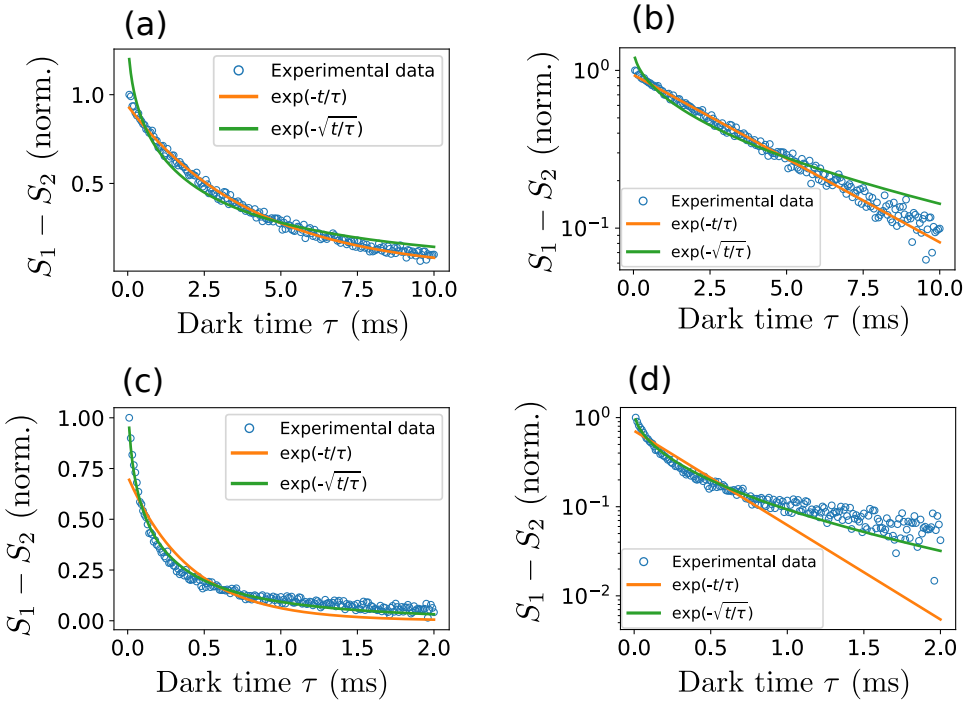

Figure 1.6: T1 measurement following the protocol described in [REF]. The best exponential and stretched exponential fits are given in every case. a) Sample CVD-pink with B≠0 and a single probed class. The optimal T_1 values are $T_1^{\text{stretch}} = 1.9$ ms and $T_1^{\text{exp}} = 4.1$ ms. b) Same measurement as a) in log scale. c) Sample ADM-15-2 with B=0. The optimal T_1 values are $T_1^{\text{stretch}} = 150$ μs and $T_1^{\text{exp}} = 410$ μs. d) Same measurement as c) in log scale.

lifetime $T_1 = 4.1$ ms comparable to the phonon-limited T_1 value of ~ 5 ms at room temperature [9].

The second spin relaxation presented in Fig. 1.6-c) and d) was performed on sample ADM-15-2 which showed a great amount of dipole-dipole spin relaxation. To further enhance the cross-relaxation rate, the experiment was performed in zero external magnetic field so that every class of NV centers would be resonant. We can observe a relaxation profile that deviates significantly from tthe exponential profile, and which is nicely fitted by a stretched exponential. The T_1 value obtained from the fit is also an order of magnetite lower than the phonon-limited value, which is coherent with the fact that dipole-dipole interactions dominate the spin relaxation in this case.

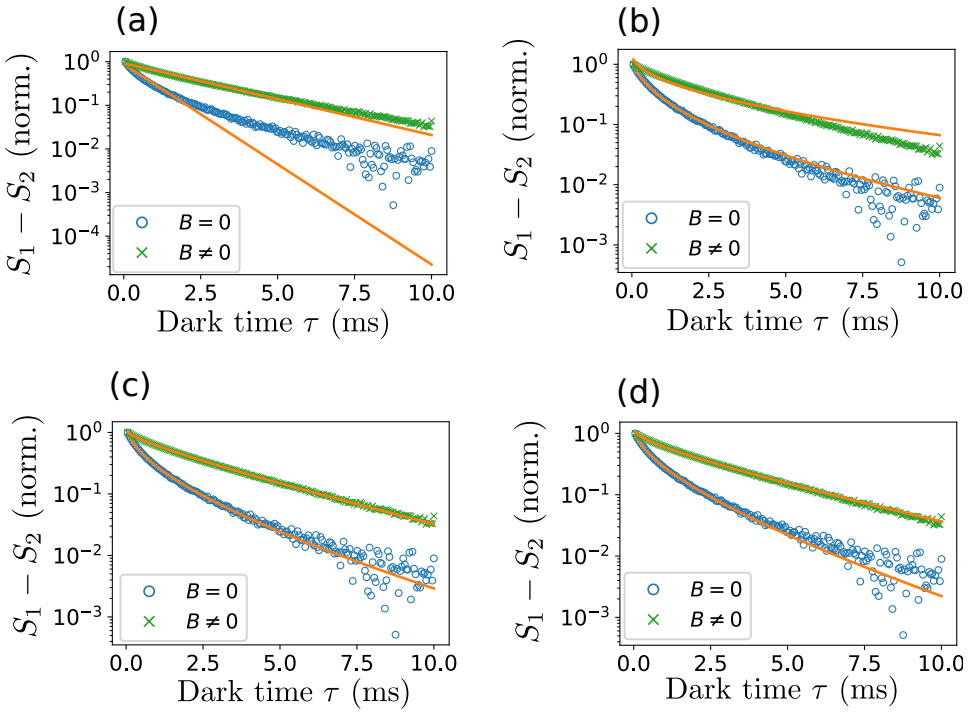

Figure 1.7: Different fitting procedure on two T_1 measurements done on sample ADM-150-1 for $B = 0$ and $B \neq 0$.
a) Exponential fit $S(\tau) = \exp\left(-\tau/T_1^{\text{ph}}\right)$.
b) Stretched exponential fit $S(\tau) = \exp\left(-\sqrt{\tau/T_1^{\text{dd}}}\right)$.
c) Bi-exponential fit $S(\tau) = \exp\left(-\tau/T_1^{\text{ph}} - \sqrt{\tau/T_1^{\text{dd}}}\right)$.
d) Bi-exponential fit with fixed $T_1^{\text{ph}} = 5$ ms: $S(\tau) = \exp\left(-\tau/5 - \sqrt{\tau/T_1^{\text{dd}}}\right)$.

1.3.2 Fitting T_1 profile in the general case

For many samples, the T_1 profile is neither fully exponential nor fully stretched exponential, because the relaxation time associated with CR, which we will call T_1^{dd}, is of the same order of magnitude as the phonon limited lifetime T_1^{ph}. Sometimes the same sample can go from mostly exponential to mostly stretched exponential depending on the number of NV-NV co-resonances, meaning that we have to include both aspects in the fitting formula.

Fig. 1.7 shows four different fitting procedure on the two same relaxation measurements. The measurements were performed on the same sample ADM-150-1, with and without an external magnetic field ($\sim 50G$). The magnetic field was strong enough to split the four classes and only one class was probed in the case $B \neq 0$, whereas all 4 classes were resonant in the

Table 1.1: Fitting parameters for Fig. 1.7. The coefficient of determination R^2 for each fit is reported here.

Figure	$B = 0$			$B \neq 0$		
	T_1^{ph} (ms)	T_1^{dd} (ms)	$1 - R^2$	T_1^{ph} (ms)	T_1^{dd}(ms)	$1 - R^2$
Fig. a)	0.95	*	$2 \cdot 10^{-2}$	2.64	*	$6 \cdot 10^{-3}$
Fig. b)	*	0.32	$2 \cdot 10^{-3}$	*	1.03	$2 \cdot 10^{-2}$
Fig. c)	6.75	0.44	$6 \cdot 10^{-4}$	4.22	7.19	$2 \cdot 10^{-4}$
Fig. d)	**5**	0.51	$6 \cdot 10^{-4}$	**5**	4.65	$6 \cdot 10^{-4}$

Bold characters indicate parameters that were arbitrarily fixed.

case $B = 0$, which strongly increases the NV-NV CR.

The fits used here are either purely exponential or purely stretched exponential, or a combination of both where the exponential lifetime T_1^{ph} was either left as a free parameter or fixed at a value $T_1^{\mathrm{ph}} = 5$ ms. The values of the different fitting parameters used is reported in Table 1.1.

We can see that neither the purely exponential nor stretched exponential fits can be satisfying for both measurements: the $B = 0$ curve is poorly fitted by the exponential fit and the $B \neq 0$ curve is poorly fitted by the stretched exponential. The protocols that include both exponential and stretched lifetimes correctly fit both curves. In the case of Fig. 1.7-d), we arbitrarily fixed $T_1^{\mathrm{ph}} = 5$ ms since this is the value we typically measure on samples with low NV density, and we expect that the phonon-limited exponential lifetime is not modified by the NV concentration.

Both the protocol where T_1^{ph} was fixed and the one where it was not correctly fit our data. We therefore decided to use the protocol where T_1^{ph} was fixed in order to minimize the number of free parameter in the fitting function. This way, the values of T_1^{dd} obtained on different measurements can be directly compared.

We should note however that the values of T_1^{dd} we obtain are not absolute. Indeed, in the case of Fig. 1.7, the value of T_1^{ph} can be somewhat arbitrarily fixed between 3 and 6 ms with satisfying fits, and the resulting values T_1^{dd} can vary by almost an order of magnitude in the case of $B \neq 0$. The values of T_1^{dd} obtained with this method have therefore to be be compared to values from the same method and the same fixed value of T_1^{ph}.

Finally, another fitting procedure is shown in Fig. 1.8. This time a single stretched exponential with an arbitrary stretch factor β is used, and satisfyingly fits the data. Fig. 1.8-b) shows the optimal β parameter as a function of the external magnetic field. It confirms that the T_1 profile gets closer to a stretched exponential ($\beta = 0.5$) when B goes to 0. Even though this method also yields satisfying fits, it employs more free parameters (β

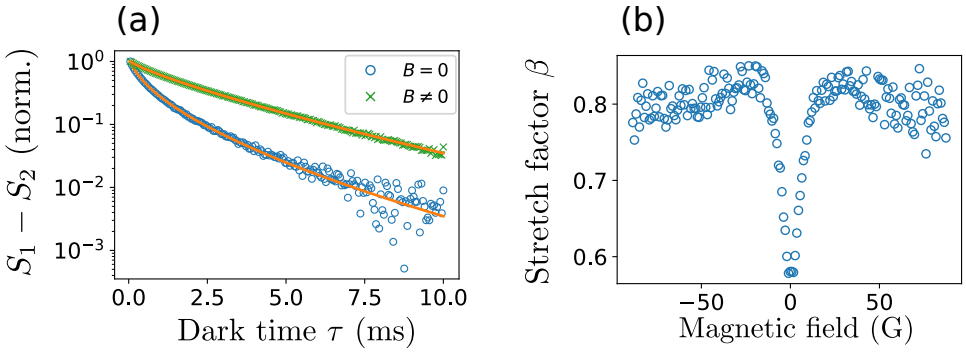

Figure 1.8: a) Same two measurements as Fig. 1.7 with the fitting formula $S(\tau) = \exp\big((-\tau/T_1)^\beta\big)$. The fitting parameters are $\beta = 0.58$ and $T_1 = 0.46$ ms for $B = 0$, and $\beta = 0.80$ and $T_1 = 2.15$ ms for $B \neq 0$. b) Optimal β parameter found for each T_1 measurement as a function of the external magnetic field (still on sample ADM-150-1).

and T_1) than the method of 1.7-d). We therefore decided to go with the later.

1.3.3 The fluctuators linewidth

The fluctuators spectral response

We now move to the second major prediction of the fluctuator model which is the spectral broadening of the fluctuators caused by the their relaxation rate γ_f. Indeed, following the arguments presented in [5], the fluctuators homogeneous spectral response is a Lorentzian of half-width $2\gamma_f$. The inhomogeneous spectral response of the ensemble of fluctuators is then further broadened by the same electric, magnetic or strain noises than the NV centers, which is characterized by $1/T_2^*$.

The fluctuator are effectively dark to ODMR measurement since they are not polarized, meaning that we cannot directly measure their linewidth as we would do for normal NV centers. We can however measure their linewidth through cross-relaxation, similarly to the detection of dark spins presented in the previous chapter.

Fig. 1.9 shows an experiment similar to the one presented in Fig. 1.2. A variable magnetic B_{scan} in addition to an offset magnetic field $B_{\text{DC}} \sim 100$ G are used in order to create a crossing between two classes of NV centers. This time however, the spin relaxation was measured instead of the PL.

Fig. 1.9-a) shows the simulated transitions of the four classes of NV centers as a function of the magnetic field. We took particular care in measuring the central frequencies of the two classes of interest (when the two lines could be clearly separated), since having a precise measurement of the detuning between the two classes $\Delta\nu$ is key to get a precise value of the

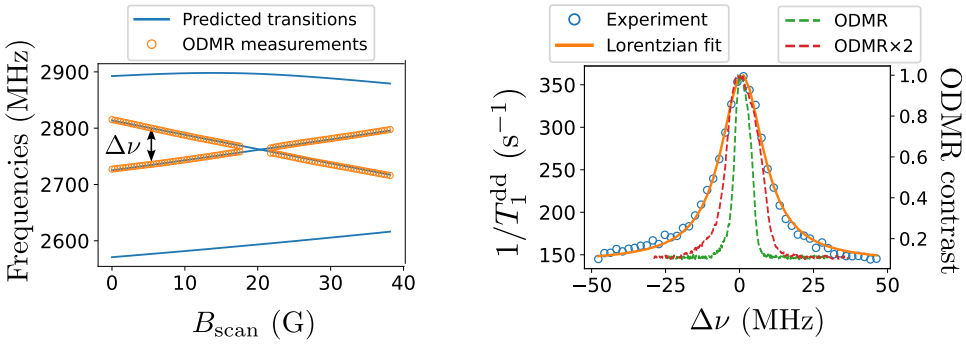

Figure 1.9: Measurement of the fluctuators linewidth on sample ADM-150-2 using the same setup as in Fig. 1.2. a) Simulation of the $|0\rangle \rightarrow |-1\rangle$ transition frequency for the four classes of NV centers and actual frequencies of the two central classes from ODMR measurements. b) Measurement of T_1^{dd} as a function of the splitting $\Delta\nu$ between the two central classes, fitted with a Lorentzian of half-width $\sigma = 8.8 \pm 0.2$ MHz. The green dashed line correspond to the ODMR spectrum of a single class of NV centers, and the red dashed one to the same line scaled up by a factor of 2

fluctuator linewidth.

Fig. 1.9-b) shows the dipole-dipole induced relaxation rate $\Gamma_1^{\text{dd}} = 1/T_1^{\text{dd}}$ as a function of the detuning $\Delta\nu$ between the two central classes. For each magnetic field value, a T_1 profile was recorded and fitted following the procedure described in Fig. 1.7-d) where we again fixed $T_1^{\text{ph}} = 5$ ms. We also show the ODMR spectrum of a single NV class for comparison.

We can clearly see that the Γ^{dd} profile is much broader than the ODMR line of the NV centers, whereas in a standard CR process, we expect the decay rate to be proportional to the spectral overlap of the two classes [27]. If we assume that both NV classes spectral response are Lorentzian of same width σ, then the spectral overlap between the two classes is also a Lorentzian of width 2σ [5]. Fig. 1.9-b) also shows the ODMR line scaled by a factor 2, which is still significantly narrower than the $1/T_1^{\text{dd}}$ line.

We attribute this broadening to the fluctuators lifetime. Another potential explanation for the broadening could be the interaction strength between the NV center and the fluctuator, but for [NV] ~ 5 ppm, the average dipole-dipole coupling strength between closest NV neighbor is $\langle \mathcal{H}_{\text{dd}} \rangle \sim 46$ kHz, which cannot explain the ~ 4 MHz broadening observed here.

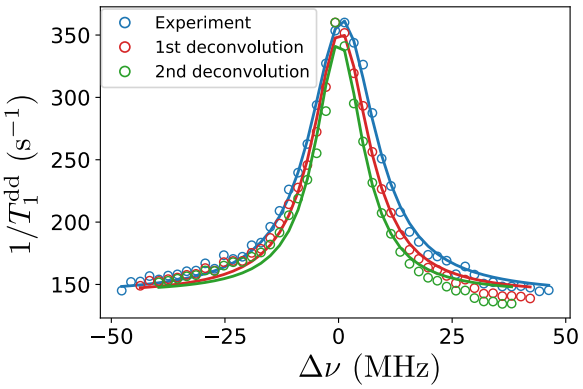

Figure 1.10: Blue curve $1/T_1^{\mathrm{dd}}$ data presented in Fig. 1.9. Red curve: deconvolution of the blue curve by the ODMR line shown on the same figure. Green curve: deconvolution of the red curve by the ODMR line. All three curves are fitted with Lorentzian of respective half widths 8.8 ± 0.2, 7.5 ± 0.3 and 6.4 ± 0.4 MHz (the precision is determined by the variance of the optimal fit parameters)

The fluctuators lifetime

We now want to extract the fluctuators lifetime $T_1^f = 1/\gamma_f$ to get further information on their potential nature.

To do this we first assume that the dipole induced decay rate is proportional to the overlap of the spectral responses of the NV centers and fluctuators S_{NV} and S_f. We will take $S_{NV}(\omega)$ and $S_f(\omega)$ as functions centered in $\omega = 0$, and consider that the spectral responses are shifted by ω_{NV}^0 and ω_f^0 respectively, the central frequencies of each group. We then have:

$$\begin{aligned}\frac{1}{T_1^{\mathrm{dd}}} &\propto \int S_{NV}(\omega - \omega_{NV}^0) S_f(\omega - \omega_f^0) d\omega \\ &= \int S_{NV}(\omega - \Delta\omega) S_f(\omega) d\omega \\ &= (S_{NV} * S_f)(\Delta\omega),\end{aligned}$$

where $\Delta\omega = \omega_{NV}^0 - \omega_f^0$.

Using the approximation $\bar{R^2} \approx (\bar{R})^2$ detailed in sec. 1.2.6, we can then decompose the fluctuator spectral response as a convolution of the lifetime contribution and the inhomogeneous broadening:

$$S_f(\omega) = \left(S_f^*(\omega)\right) * \left(\frac{1}{1 + \left(\frac{\omega}{2\gamma_f}\right)^2}\right), \tag{1.14}$$

[5]For other line profile, the overlap would be smaller than 2σ. For instances, the overlap of two Gaussians of width σ is a Gaussian of width $\sqrt{2}\sigma$

where S_f^* is the spectral broadening caused by the inhomogeneous distribution of the fluctuators, which we will suppose to be equal to S_{NV}. With these assumptions, we are now ready to extract γ_f from the data of Fig. 1.9.

The first way to do this, as was done for NV-P1 CR in [27], is to deconvolve the $1/T_1^{\text{dd}}$ data by the ODMR spectrum using a Wiener deconvolution algorithm. The result of the deconvolution is shown in Fig. 1.10: the data is deconvolved once to get the spectral response of the fluctuator (red curve), and a second time to get only the lifetime contribution of the fluctuator (green curve). Fitting with Lorentzians, we find a final value $\Gamma_2 = 2\gamma_f = (2\pi)6.4 \pm 0.4$ MHz which corresponds to a fluctuator lifetime $T_1^f = \frac{1}{\gamma_f} = 50 \pm 3$ ns[6].

Another, simpler alternative is to consider that the $1/T_1^{\text{dd}}$ profile is a Voigt profile given by the convolution of two Gaussians of half width at half maximum (HWHM) $f_G = \frac{\sqrt{\ln(2)}}{\pi T_2^*}$ and a Lorentzian of HWHM $f_L = \frac{2\gamma_f}{2\pi}$:

$$\begin{aligned}\Gamma_1^{\text{dd}} &\propto \mathcal{G}(f_G) * (\mathcal{L}(f_L) * \mathcal{G}(f_G)) \\ &\propto \mathcal{L}(f_L) * \mathcal{G}(\sqrt{2} f_G),\end{aligned}$$

where $\mathcal{G}(f_G)$ and $\mathcal{L}(f_L)$ denote Gaussian and Lorentzian functions of HWHM f_G and f_L respectively. We can then use the formula of a pseudo-Voigt profile which gives an approximation of the Voigt profile's HWHM f as a function of f_G and f_L [28]:

$$f = [f_G^5 + 2.69269 f_G^4 f_L + 2.42843 f_G^3 f_L^2 + 4.47163 f_G^2 f_L^3 + 0.07842 f_G f_L^4 + f_L^5]^{1/5}. \tag{1.15}$$

With $f = 8.8 \pm 0.2$ MHz and $\sqrt{2} f_G = 4.3 \pm 0.2$ MHz, we find $f_L = 6.5 \pm 0.3$ MHz for a final lifetime value $T_1^f = 49 \pm 2$ ns, a value consistent with the one found with the deconvolution method.

Doing similar experiments and calculations, [5] found $\gamma_f = 1/T_1^f = (2\pi)3.3$ MHz which gives them a fluctuator lifetime value $T_1^f = 48$ ns, a value very close to the ones we obtained above, despite using a completely different sample.

In conclusion, we observed that the fluctuators linewidth was indeed broadened by their relaxation rate which justifies the initial hypothesis that $T_1^f \ll T_1^{NV}$. It even shows that T_1^f is of the same order of magnitude as the optical lifetime (~ 15 ns) which explains why the fluctuators cannot be optically polarized.

[6] We define here the fluctuators lifetime T_1^f as $\frac{1}{\gamma_f}$ for simplicity, but it should be noted that the actual lifetime of the fluctuators states is $\frac{1}{2\gamma_f}$ due to the competition between the two possible decay channels for each state (cf Fig. 1.4).

1.4 Resonance between several NV classes

The main tool to probe NV-NV CR is to use the co-resonances between the NV classes. While it is not possible to completely shut down the CR, because the NV centers from the same class are always resonant with each other, we can tune the density of resonant NV centers (and resonant fluctuators) by a factor of 4 by playing with the inter-class co-resonances. In this section, we will discuss the various scenarios where NV classes overlap, and quantify theoretically and experimentally the dipole-induced relaxation rate in each case.

1.4.1 Geometric conditions for inter-class resonance

There are four possibilities to obtain inter-class resonance (aside from the non-equivalent CR discussed in sec. 1.1.1). These possibilities are:

- $\mathbf{B} \in \{110\}$. We refer by $\{110\}$ as any plane orthogonal to a $\langle 110 \rangle$ or equivalent direction. In this magnetic configuration, two classes are at resonance and the two other ones are spectrally isolated.
- $\mathbf{B} \in \{100\}$. In this magnetic configuration, the four classes form two pairs of co-resonance.
- $\mathbf{B} \parallel \langle 111 \rangle$. In this configuration discussed in the last chapter, one class is aligned with the magnetic field and is spectrally isolated while the three other form a resonant triplet.
- $\mathbf{B} \parallel \langle 100 \rangle$. In this configuration also discussed in the last chapter, the four classes are resonant.

We should add to this list the case $\mathbf{B} = 0$ where all four classes are also resonant, and any other possibility (which we will label random $\mathbf{B}$) where all four classes are spectrally separated.

An ODMR spectrum and a representation of the magnetic field in the diamond unit cell for each of these six possibilities is shown in Fig. 1.11.

This relation between NV-NV class resonances and the magnetic field being in specific crystalline planes or directions means that we can determine the crystal main axes simply by PL experiments.

Fig. 1.12 shows a map where we monitored the PL of sample CVD-pink while scanning the magnetic field angle around the [001] axis, thanks to a permanent magnet on a motorized goniometer. We have also reported the locus of $\mathbf{B}$ being in the planes [100], [010], [110] and $[1\bar{1}0]$.

We know that when $\mathbf{B}$ belongs to any of these four planes, there is a co-resonance between at least two NV classes. This co-resonance leads to an increase in NV-NV CR and a faster depolarization of the spins involved, which ultimately leads to a drop in PL. We can indeed see in fig. 1.12 that

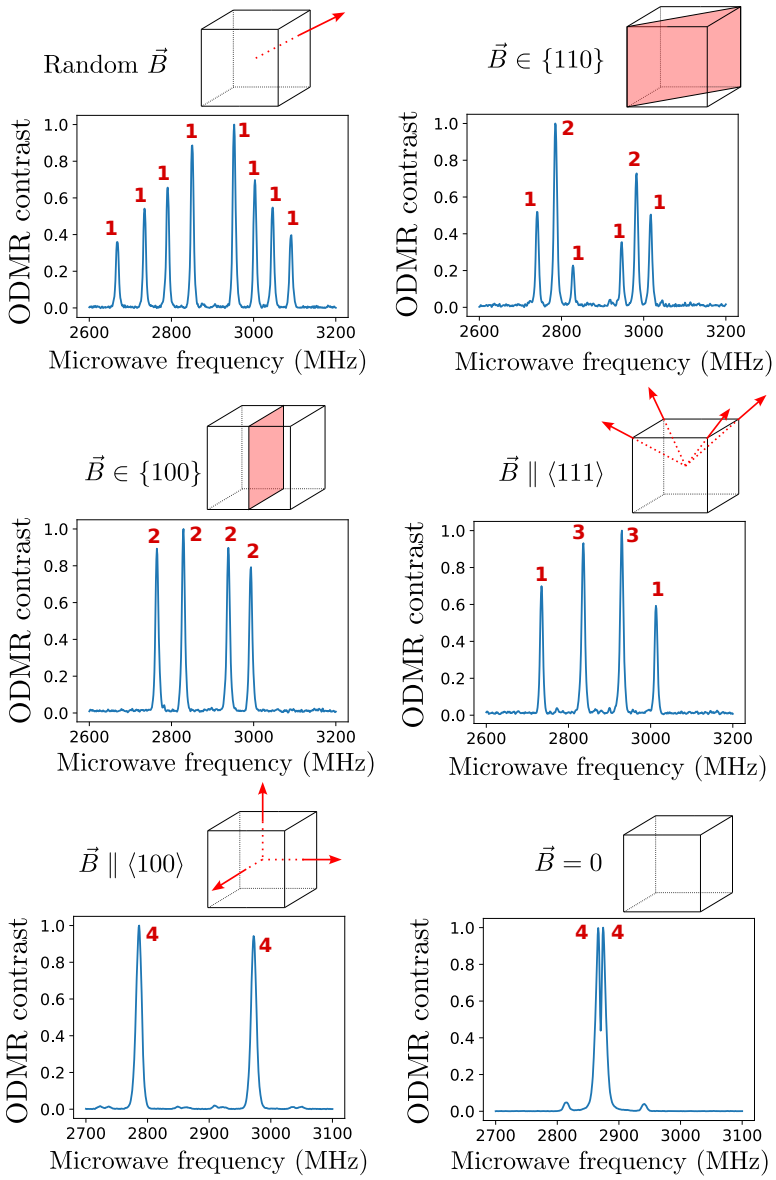

Figure 1.11: ODMR spectra on sample ADM-15-3 as a function of the magnetic field orientation. The field amplitude is $\sim$ 60 G. Red numbers represent the number of resonant classes for each ODMR line. The cubes represent the diamond unit cell, and the red planes/arrow the possible orientations of the magnetic field

there is clear correlation between the loci of **B** and drops in PL. We can also see that the PL is at its lowest when **B** $\parallel$ [001], which corresponds to a four class degeneracy.

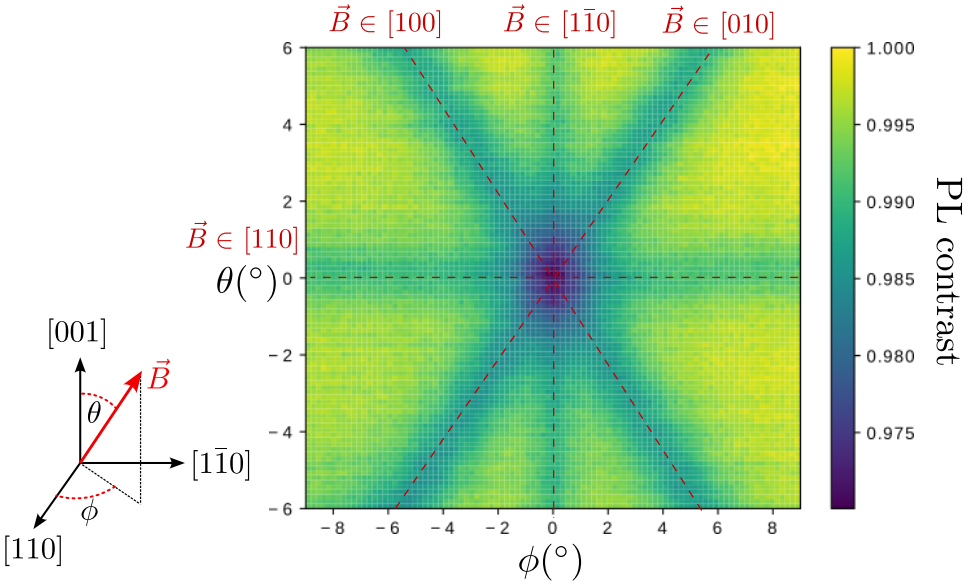

Figure 1.12: PL contrast as a function of the magnetic field polar and azimuthal angle with respect to the [100] axis on sample CVD-pink. The field amplitude is $|B| \sim 115G$. The locus of the magnetic field in specific planes is noted by red dashed lines.

1.4.2 Quantitative modification of T_1

The fluctuator model allows quantitative predictions of the change in the spin lifetime, thanks to eq. 1.7. There are however several unknowns in this equation, such as the fluctuator density and lifetime which can be hard to estimate. It is however relatively easy to compare the predictions of eq. 1.7 for various magnetic field configurations.

We decided to take the case of an isolated class as the baseline value for the dipole-dipole decay rate Γ_0, and to express the decay rates when 2, 3 or 4 classes are co-resonant as a function of Γ_0. Doing so allows us to normalize n_f and γ_f in eq. 1.7 and to keep $\bar{G}$ the geometrical part of $\bar{\eta}$ as the only unknown.

$\bar{G}$ can be analytically or numerically computed for each of the magnetic configurations listed before, as detailed in appendix [REF]. This allows us to predict the value of the spin decay rate in every situations as a function of the decay rate of an isolated class.

Table 1.2 shows these predicted values, along with experimental ones on sample ADM-15-3. The experimental values were obtained with the protocol described in Fig. 1.7-d) with a double exponential fit where we fixed again $T_1^{\mathrm{dd}} = 5$ ms.

The theoretical values are in a good qualitative agreement with the experimental ones, both ranking the different scenarios in the same order. The

Table 1.2: Theoretical and experimental values of $\Gamma_1^{\mathrm{dd}} = 1/T_1^{\mathrm{dd}}$ for various magnetic field configurations, expressed as a function of the value found for an isolated class. The experimental values were measured on sample ADM-15-3 using the protocol of Fig. 1.7-d) with $T_1^{\mathrm{ph}} = 5$ ms. The uncertainty corresponds to the precision of the fit parameters.

$\Gamma_1^{\mathrm{dd}}(\mathbf{B})$	Theory	Experimental
random $\mathbf{B}$ (1 class)	Γ_0^{th}	1.53 ± 0.04 ms$^{-1} \equiv \Gamma_0^{\mathrm{exp}}$
$\mathbf{B} \in \{110\}$ (2 classes)	10.0 Γ_0^{th}	5.2 ± 0.1 Γ_0^{exp}
$\mathbf{B} \in \{100\}$ (2 classes)	7.24 Γ_0^{th}	4.2 ± 0.1 Γ_0^{exp}
$\mathbf{B} \parallel \langle 111 \rangle$ (3 classes)	28.4 Γ_0^{th}	11.6 ± 0.4 Γ_0^{exp}
$\mathbf{B} \parallel \langle 100 \rangle$ (4 classes)	42.8 Γ_0^{th}	14.1 ± 0.5 Γ_0^{exp}
$\mathbf{B} = 0$ (4 classes)	51+(*) Γ_0^{th}	19.9 ± 0.8 Γ_0^{exp}

(*) The case $\mathbf{B} = 0$ will be detailed in the next chapter. The theoretical value is a lower bond.

quantitative predictions of the theory however are rather poor, being off by more than a factor of 3 for the shortest lifetimes.

It should be noted that the experimental values were heavily influenced by the choice of the parameter T_1^{ph}. Using for example $T_1^{\mathrm{ph}} = 2.5$ ms gave results closer to the theoretical ones. Nevertheless, the fluctuator model generally tends to overestimate the depolarization rates.The authors of [5] for instance found that a 2-class degeneracy (the authors did not precise whether this was a $\mathbf{B} \in \{110\}$ or $\mathbf{B} \in \{100\}$ configuration) yielded an increased depolarization rate by a factor ~ 4, a value comparable to the one we found in table 1.2, and two times smaller than the predicted one[7].

The failure of the fluctuator model to accurately predict the changes in T_1 is one of the reasons that led us to believe that the model is incomplete. Other reasons will be presented in the following part.

1.5 Conclusion and perspectives

In conclusion, we have seen in this chapter that dense NV ensemble present "anormal" CR between the NV centers, and we have shown how the fluctuator model developed by Choi et al. in [5] can explain this behavior. The fluctuator model not only explains the NV-NV CR, but also correctly predicts the stretched exponential lifetime profile. It also correctly predicts that the fluctuators have a broader spectral response than the other NV centers. Nevertheless, the model does not describe perfectly every aspects of NV-NV relaxation, and there still are many aspects of this problem, both

[7] We can also see in Fig. 1.9 that a $\mathbf{B} \in \{110\}$ configuration leads to a ~ 2.5 times increase in Γ_1^{dd}, which is 4 times smaller than the predicted factor of 10.

theoretical and experimental, to explore.

In what follows we will describe what could be interesting investigation points to further understand the NV-NV relaxation and the fluctuator model.

1.5.1 Limitations of the fluctuator model

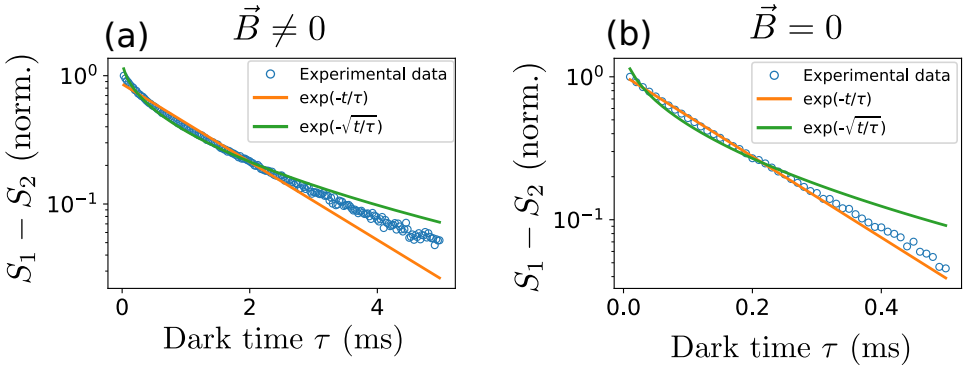

Figure 1.13: T_1 measurements on sample ADM-15-4, fitted with pure exponential or stretched exponential. a) T_1 of a single isolated class when $\mathbf{B} \neq 0$. The optimal fit parameters are respectively $T_1^{\text{exp}} = 1.43$ ms and $T_1^{\text{stretch}} = 0.56$ ms. b) T_1 of the four degenerate classes when $\mathbf{B} = 0$. The optimal fit parameters are respectively $T_1^{\text{exp}} = 0.15$ ms and $T_1^{\text{stretch}} = 0.05$ ms.

We mentioned previously that the discrepancy between the theoretical and experimental T_1 values were in contradiction with the current fluctuator model, although the difference could come in part from the T_1 fitting procedure. Another, more glaring problem is the fact that some T_1 profile are not stretched exponential.

Fig. 1.13 shows T_1 measurement on sample ADM-15-4, either on a single isolated class ,where the dipole-dipole interactions are at their weakest, or on all four resonant classes at $\mathbf{B} = 0$, where the interactions are at their strongest.

Although the spin lifetime still gets ~ 10 times shorter in the $\mathbf{B} = 0$ case, indicating that dipole-dipole interaction still plays an important role in the spin relaxation, this time the lifetime profile does not converge to a purely stretched exponential. In fact it seems to be the opposite: the lifetime profile is closer to a pure exponential for the shorter T_1 (especially for the very short times), and closer to a stretched exponential for the longer T_1, which is in complete contradiction with the fluctuator model and the previous observations in Fig. 1.6 and 1.7.

We should note that most sample studied follow the fluctuator model, in that the their lifetime profile gets closer to a stretched exponential when the dipole-dipole relaxation rate is increased. Sample ADM-15-4 seem to

be an anomaly in this regard, since most of the samples from the same batch (including sample ADM-15-2 in Fig. 1.6) seem to follow the "normal" behavior predicted by the fluctuator model. However, some other samples, including bulk HPHT samples and 150 μm Adamas micro-diamond also showed short (non stretched) exponential lifetimes.

It seems therefore that the current fluctuator model does not correctly describe the spin dynamics of every NV-dense samples. Looking at what was previously done for P-doped SI [18] or for FRET [25], the fluctuator model could probably be improved by taking into account the finite lifetime of the fluctuators (i.e. the saturation of the NV-fluctuator CR), and the spin diffusion between NV centers (the fluctuator model only considers NV-fluctator interactions and not NV-NV interactions).

1.5.2 Investigation of the fluctuators nature

While the hypothesis of fluctuators being clusters of NV centers or NV-other spins is strengthened by the precedents in P-doped Si [15] or F centers in KCl [29], there are still many unknowns on the exact nature of the fluctuators. There are at least two aspects that merit to be investigated.

The first one would be to study the fluctuator spectral profile on various samples showing NV-NV CR. In particular it would be interesting to know whether this profile is always Lorentzian, and what its linewidth is. In the sample studied on Fig. 1.9, we found a value for γ_f surprisingly similar to the one found in [5], even tough our sample only had [NV] $\sim$ 3ppm compared to the [NV] $\sim$ 15ppm sample used in [5] [8]. If γ_f was found to be somewhat of a constant among all samples showing NV-NV CR, this would give us a lot of information on the potential nature of the fluctuators. Studying the temperature dependency of γ_f could also give us information on whether the depolarization mechanism is due to tunneling or modulation of the $J-$coupling by the phonons.

The other aspect would be to identify potential defects that could form fluctuators when paired with NV centers. The main candidate for this would be substitutional nitrogen (P1 or $P1^+$ centers) since they are the most abundant electronic spin species in the diamond we use. The ideal way to confirm this hypothesis would be to compare the spin T_1 for different samples with the same [NV] concentration, but different [P1] concentration. If indeed P1 centers play a role in the presence of fluctuators, we would expect a shorter NV T_1 time in the sample with high P1 concentration.

[8] Although the initial paper claimed a NV concentration [NV] $\sim$ 45ppm, a more recent paper re-established the concentration at $\sim 45 ppm$ [1]

Bibliography

[1] Hengyun Zhou et al. "Quantum metrology with strongly interacting spin systems". In: *Physical review X* 10.3 (2020), p. 031003.

[2] Soonwon Choi et al. "Observation of discrete time-crystalline order in a disordered dipolar many-body system". In: *Nature* 543.7644 (2017), pp. 221–225.

[3] Georg Kucsko et al. "Critical thermalization of a disordered dipolar spin system in diamond". In: *Physical review letters* 121.2 (2018), p. 023601.

[4] Chong Zu et al. "Emergent hydrodynamics in a strongly interacting dipolar spin ensemble". In: *Nature* 597.7874 (2021), pp. 45–50.

[5] Joonhee Choi et al. "Depolarization dynamics in a strongly interacting solid-state spin ensemble". In: *Physical review letters* 118.9 (2017), p. 093601.

[6] Seiji Armstrong et al. "NV–NV electron–electron spin and NV–NS electron—electron and electron-nuclear spin interaction in diamond". In: *Physics Procedia* 3.4 (2010), pp. 1569–1575.

[7] K Holliday et al. "Optical hole-bleaching by level anti-crossing and cross relaxation in the NV centre in diamond". In: *Journal of Physics: Condensed Matter* 1.39 (1989), p. 7093.

[8] Eric van Oort and Max Glasbeek. "Cross-relaxation dynamics of optically excited N-V centers in diamond". In: *Physical Review B* 40.10 (1989), p. 6509.

[9] A Jarmola et al. "Temperature-and magnetic-field-dependent longitudinal spin relaxation in nitrogen-vacancy ensembles in diamond". In: *Physical review letters* 108.19 (2012), p. 197601.

[10] Mariusz Mrózek et al. "Longitudinal spin relaxation in nitrogen-vacancy ensembles in diamond". In: *EPJ Quantum Technology* 2 (2015), pp. 1–11.

[11] A Jarmola et al. "Longitudinal spin-relaxation in nitrogen-vacancy centers in electron irradiated diamond". In: *Applied Physics Letters* 107.24 (2015), p. 242403.

[12] Rinat Akhmedzhanov et al. “Microwave-free magnetometry based on cross-relaxation resonances in diamond nitrogen-vacancy centers”. In: *Physical Review A* 96.1 (2017), p. 013806.

[13] R Giri et al. “Coupled charge and spin dynamics in high-density ensembles of nitrogen-vacancy centers in diamond”. In: *Physical Review B* 98.4 (2018), p. 045401.

[14] G Feher and EA Gere. “Electron spin resonance experiments on donors in silicon. II. Electron spin relaxation effects”. In: *Physical Review* 114.5 (1959), p. 1245.

[15] A Honig and E Stupp. “Electron spin-lattice relaxation in phosphorus-doped silicon”. In: *Physical Review* 117.1 (1960), p. 69.

[16] Ko Sugihara. “Spin-Lattice Relaxation of Shallow Donors in Heavily Doped Si”. In: *Journal of the Physical Society of Japan* 18.7 (1963), pp. 961–969.

[17] G Yang and A Honig. “Concentration-and Compensation-Dependent Spin-Lattice Relaxation in N-Type Silicon”. In: *Physical Review* 168.2 (1968), p. 271.

[18] BE Vugmeister. “Spin diffusion and spin–lattice relaxation in paramagnetic crystals”. In: *physica status solidi (b)* 90.2 (1978), pp. 711–718.

[19] GP Berman et al. “Spin diffusion and relaxation in a nonuniform magnetic field”. In: *Physical Review B* 71.18 (2005), p. 184409.

[20] Nicolaas Bloembergen. “On the interaction of nuclear spins in a crystalline lattice”. In: *Physica* 15.3-4 (1949), pp. 386–426.

[21] PG De Gennes. “Sur la relaxation nucleaire dans les cristaux ioniques”. In: *Journal of Physics and Chemistry of Solids* 7.4 (1958), pp. 345–350.

[22] WE Blumberg. “Nuclear spin-lattice relaxation caused by paramagnetic impurities”. In: *Physical Review* 119.1 (1960), p. 79.

[23] Theodor Förster. “Experimentelle und theoretische Untersuchung des zwischenmolekularen Übergangs von Elektronenanregungsenergie”. In: *Zeitschrift für naturforschung A* 4.5 (1949), pp. 321–327.

[24] KB Eisenthal and S Siegel. “Influence of resonance transfer on luminescence decay”. In: *The Journal of Chemical Physics* 41.3 (1964), pp. 652–655.

[25] Mario Yokota and Osamu Tanimoto. “Effects of diffusion on energy transfer by resonance”. In: *Journal of the physical society of Japan* 22.3 (1967), pp. 779–784.

[26] Neil B Manson et al. “NV—N+ pair centre in 1b diamond”. In: *New Journal of Physics* 20.11 (2018), p. 113037.

[27] LT Hall et al. “Detection of nanoscale electron spin resonance spectra demonstrated using nitrogen-vacancy centre probes in diamond”. In: *Nature communications* 7.1 (2016), pp. 1–9.

[28] T Ida, M Ando, and H Toraya. “Extended pseudo-Voigt function for approximating the Voigt profile”. In: *Journal of Applied Crystallography* 33.6 (2000), pp. 1311–1316.

[29] Roger W Warren, DW Feldman, and JG Castle Jr. “Spin-lattice relaxation of F centers in KCl: interacting F centers”. In: *Physical Review* 136.5A (1964), A1347.